

### b) Circular Lattice

For a circular accelerator, the periodicity is usually taken to be not the superperiodicity of the machine (i.e. the number of identical lattice sections), but the revolution period. The index  $n$  therefore represents turn number. The mismatch  $B_{mag}$  most often arises from improper orientation of the beam ellipse at injection. Neglecting the static phase offset  $\chi(x^2)_0$  in Eq. (3.63), the equilibrium emittance is

$$\epsilon_n = \frac{\langle x^2 \rangle_n}{\beta} = \epsilon_0 [B_{mag} + \sqrt{B_{mag}^2 - 1}] \cos(4\pi n), \quad (3.69)$$

where the phase advance per turn is  $\nu = 2\pi\psi$ . Shown in Fig. 3.22 is the evolution of the transverse phase space for  $B_{mag}$  along with the projections onto the horizontal axis. With a turn-by-turn beam size monitor, the consequences of a mismatch can be measured directly by detecting the beam size changes at every turn.

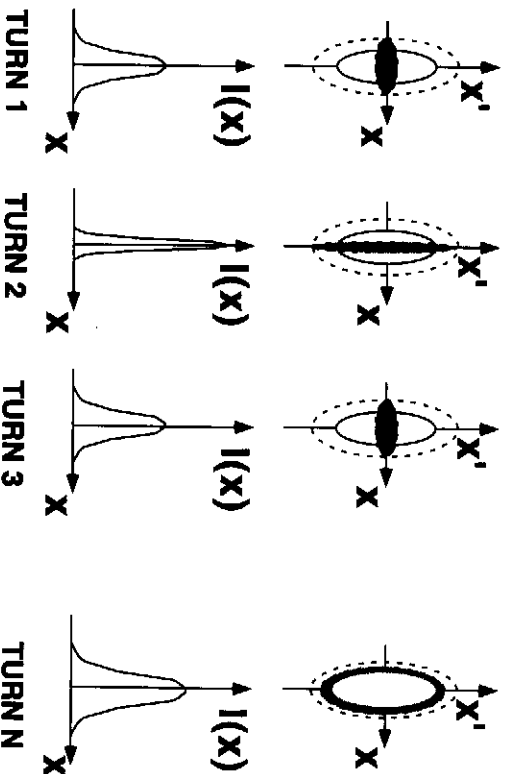


Figure 3.22: Horizontal phase space and  $x$ -projection for a mismatched beam in a circular accelerator.

### 3.3 Beta Matching in a Transport Line or Linac

The beam size (squared) at the location  $s$  can be expressed in terms of the  $\alpha$  and  $\beta$  functions and the emittance at an upstream location  $s_0$  as

$$\langle x^2(s) \rangle = R_{11}^2 \beta(s_0) \epsilon - 2R_{12} R_{11} \alpha(s_0) \epsilon + R_{12}^2 \gamma(s_0) \epsilon \quad (3.70)$$

In a quadrupole scan, the transfer matrix elements  $R_{11}$  and  $R_{12}$  are varied, by changing the strength of a quadrupole between  $s_0$  and  $s$ . Beam-size measurements for at least 3 different quadrupole settings are required in order to solve for the three independent unknown parameters:  $\epsilon$ ,  $\beta(s_0)$  and  $\alpha(s_0)$ . The fourth parameter,  $\gamma(s_0)$  is not free, but determined by  $\alpha(s_0)$  and  $\beta(s_0)$ :  $\gamma = (1 + \alpha^2)/\beta$ .

A multi-wire (or multi-screen) emittance measurement is very similar. Here, the quadrupole gradients stay constant, but the  $R$  matrices between  $s_0$  and the different wire scanners (or other beam-size monitors) are different. Again, at least 3 measurements are required.

Either case can be described by a matrix equation of the form:

$$\begin{pmatrix} \sigma_x^{(1)2} \\ \sigma_x^{(2)2} \\ \sigma_x^{(3)2} \\ \dots \\ \sigma_x^{(n)2} \end{pmatrix} = \begin{pmatrix} R_{11}^{(1)2} & 2R_{11}^{(1)}R_{12}^{(1)} & R_{12}^{(1)2} \\ R_{11}^{(2)2} & 2R_{11}^{(2)}R_{12}^{(2)} & R_{12}^{(2)2} \\ R_{11}^{(3)2} & 2R_{11}^{(3)}R_{12}^{(3)} & R_{12}^{(3)2} \\ \dots & \dots & \dots \\ R_{11}^{(n)2} & 2R_{11}^{(n)}R_{12}^{(n)} & R_{12}^{(n)2} \end{pmatrix} \begin{pmatrix} \beta(s_0)\epsilon \\ -\alpha(s_0)\epsilon \\ \gamma(s_0)\epsilon \end{pmatrix} \quad (3.71)$$

where the superindex on the right hand-side refers to the different measurements, *i.e.*, it either corresponds to the setting of some quadrupole magnet, in case of a quadrupole scan, or to a different wire scanner or monitor, in case of a multi-wire emittance measurement. At least 3 measurements are required ( $N \geq 3$ ) in order to solve for the three independent parameters  $\epsilon$ ,  $\beta(s_0)$  and  $\alpha(s_0)$ .

To simplify the notation, let us denote the  $n \times 3$  matrix on the right-hand side of Eq. (3.71) as  $\mathbf{B}$ , the  $n$ -component vector on the left side by  $\Sigma_x = (\sigma_x^{(1)2}, \dots, \sigma_x^{(n)2})$ , and the 3-component vector on the far right by

$$\mathbf{o} = (\beta(s_0)\epsilon, -\alpha(s_0)\epsilon, \gamma(s_0)\epsilon). \quad (3.72)$$

The equation then reads:

$$\Sigma_x = \mathbf{B} \cdot \mathbf{o} \quad (3.73)$$

The problem of determining the elements of the vector  $\mathbf{o}$  can be solved by a simple least-squares fit. We have to minimize the sum

$$\chi^2 = \sum_{i=1}^n \frac{1}{\sigma_{\Sigma_x^{(i)}}^2} \left( \Sigma_x^{(i)} - \sum_{i=1}^3 B_{ii} o_i \right)^2 \quad (3.74)$$

where  $\sigma_{\Sigma_x^{(i)}}$  denotes the rms error of  $\Sigma_x^{(i)} = \sigma_x^{(i)2}$ . This error is obtained from the fit to the  $i$ th wire scan which determines the rms beam size  $\sigma_x^{(i)}$ .

We find it convenient to normalize the coordinates  $\Sigma^{(l)}$  so that the rms error is 1:

$$\hat{\Sigma}_x^{(l)} = \frac{\Sigma_x^{(l)}}{\sigma_{\Sigma_x^{(l)}}} \quad (3.75)$$

$$\hat{B}_{ii} = \frac{B_{ii}}{\sigma_{\Sigma_x^{(l)}}} \quad (3.76)$$

Forming a symmetric  $n \times n$  covariance matrix

$$\mathbf{T} = (\hat{\mathbf{B}}^T \cdot \hat{\mathbf{B}})^{-1} \quad (3.77)$$

the least-squares solution to Eq. (3.73) reads:

$$\mathbf{o} = \mathbf{T} \cdot \hat{\mathbf{B}}^T \cdot \hat{\Sigma}_x^{(l)} \quad (3.78)$$

and the error of any scalar function  $f(\mathbf{o})$  is given by

$$\sigma(f)^2 = (\nabla_{\mathbf{o}} f)^T \cdot \mathbf{T} \cdot (\nabla_{\mathbf{o}} f). \quad (3.79)$$

In particular, the errors of the parameters  $\mathbf{o}$  themselves are

$$\sigma_{o_i} = \sqrt{T_{ii}} \quad (3.80)$$

Once the components of  $\mathbf{o}$  are known, we still need to perform a simple nonlinear transformation to infer  $\epsilon$ ,  $\beta$ , and  $\alpha$ :

$$\epsilon = \sqrt{o_1 o_3 - o_2^2} \quad (3.81)$$

$$\beta = o_1 / \epsilon \quad (3.82)$$

$$\alpha = -o_2 / \epsilon \quad (3.83)$$

The error propagation is straightforward, using Eq. (3.79).

The deviation of the  $\beta$ ,  $\alpha$ , and  $\gamma$  from the design parameters  $\beta_0$ ,  $\alpha_0$  and  $\gamma_0$  is often characterized in terms of the 'B<sub>mag</sub>' ( $\beta$  matching) parameter<sup>27,28</sup>:

$$B_{mag} = \frac{1}{2} (\beta\gamma_0 - 2\alpha\alpha_0 + \gamma\beta_0) \quad (3.84)$$

The parameter  $B_{mag}$  has an important physical meaning. If a beam is injected into a ring or linac with a mismatch, the beam will filament until its distribution approaches a shape that is matched to the ring or the linac lattice. However, the filamentation causes the beam emittance to increase, such that, after complete filamentation, the emittance is given by the product of  $B_{mag}$  and the initial value of  $\epsilon$ .

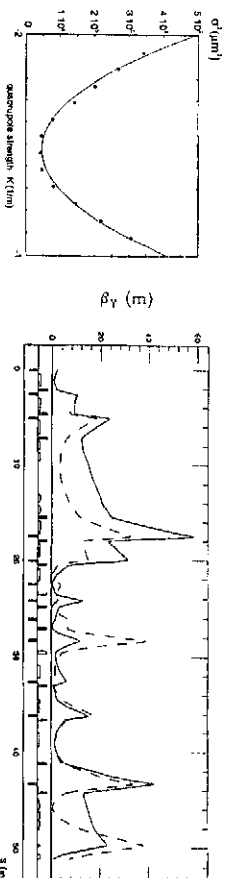


Figure 3.23: Beta matching in the KEK/ATF-BT<sup>29</sup>: (left) quadrupole-scan emittance measurement; shown is the square of the vertical beam size on a profile monitor vs. the strength of an upstream quadrupole; (right) the vertical beta function obtained by propagating the measured twiss parameters (solid) through the actual BT optics is compared with the beta function expected for the design optics (dashed).

### Ex.3.2. Beta mismatch

Suppose a beam is injected with a distribution characterized by optical functions  $\beta$ ,  $\alpha$  and  $\gamma$  different from the matched values  $\beta_0$ ,  $\alpha_0$  and  $\gamma_0$ . Show that the beam emittance after filamentation is given by  $\epsilon = B_{mag} \epsilon_0$ , where  $\epsilon_0$  is the initial emittance of the injected beam, and  $B_{mag}$  was defined in Eq. (3.84). Hint: filamentation corresponds to a randomization of the betatron phase and  $\epsilon = \langle I \rangle$ .

Once the values of  $\beta$  and  $\alpha$  are known, quadrupole magnets can be adjusted so as to match the optical functions at a selected point to their design value, which is equivalent to  $B_{mag}=1$ . The above procedure also provides an absolute measure of the emittance. The SLC has more than 10 multi-wire emittance measurement stations, which monitor the beam emittances in various parts of the machine in hourly intervals, and are indispensable for emittance control and tuning. For example, in the SLC linac transverse orbit bumps are intentionally induced as a global correction which cancels the accumulated local effects of dispersion or wakefields. The bumps are optimized by minimizing the emittance downstream, as calculated by this measurement technique.

### Example

To illustrate the beta matching method, Fig. 3.23 shows an example from the KEK/ATF beam transport line (BT), connecting the S-band linac and the ATF damping ring. The left picture shows the result of a typical quadrupole scan at the end of the BT. Plotted is the square of the vertical beam size versus the strength of an upstream quadrupole, as well as a quadratic fit to the data. We can propagate the twiss parameters deduced from such a fit through the BT, using a model derived from the actual or the design magnet settings. The right picture displays the inferred beta functions.

**Ex.3.1. Design of an orbit feedback loop** Write an algorithm for orbit correction in one plane assuming uncoupled, linear transport in a transport line. Let the beam position be detected using two BPMs and use two fast corrector dipoles for implementing the desired deflections. Introduce (assumed known) relative phase advances and beta functions as needed to take into account phase differences between the correctors, between the BPMs, and between the correctors and BPMs.

### 3.2 Beam Emittance and Emittance Preservation

The beam emittance represents the volume of the beam occupied in the six dimensional phase space  $(x, x', y, y', \phi, \delta)$ , where  $x$  and  $y$  are the transverse positions,  $x'$  and  $y'$  are the transverse angles,  $\phi$  is the time-like variable representing the relative phase of the beam, and  $\delta$  is the relative beam energy. Often one discusses a beam emittance with implicit reference to a particular plane of interest; i.e. the horizontal, vertical, or longitudinal emittance. In this section we describe not single particle transport, but transport of the beam as a whole. Next we outline methods used to measure the beam emittance and to parametrize the degree of mismatch using very commonly used wire scanners.

#### 3.2.1 Single Wire Measurement of Beam Emittance

An (invasive<sup>b</sup>) measurement of the beam emittance can be performed by varying the field strength of a quadrupole located upstream of a single wire (or screen). The transfer matrix is  $M = SQ$ , where  $S$  is the known transfer matrix between the quadrupole and the wire, and  $Q$  is the transfer matrix of the quadrupole:

$$Q = \begin{pmatrix} 1 & 0 \\ k = \pm \frac{1}{f} & 1 \end{pmatrix} \quad (3.21)$$

in the thin-lens approximation for which the length of the quad is short compared to the focal length  $f$ . After multiplying the matrices, one obtains

$$M = \begin{pmatrix} S_{11} + kS_{12} & S_{12} \\ S_{21} + kS_{22} & S_{22} \end{pmatrix}. \quad (3.22)$$

Expanding the matrix product  $\sigma = (SQ)\sigma_0(SQ)^T$  and equating the (11) element on both sides, the horizontal beam size is

<sup>b</sup>The measurement could be made noninvasive by simultaneously adjusting another quadrupole downstream of the wire scanner, so as to compensate for the change in the beta function induced by the first quadrupole

$$\begin{aligned}\sigma_{11}(\langle x^2 \rangle) &= (S_{11}^2 \sigma_{11_0} + 2S_{11} S_{12} \sigma_{12_0} + S_{12}^2 \sigma_{22_0}) \\ &+ (2S_{11} S_{12} \sigma_{11_0} + 2S_{12}^2 \sigma_{12_0})k + S_{12}^2 \sigma_{11} k^2, \quad (3.23)\end{aligned}$$

which is quadratic in the field parameter  $k$ .

To make use of these results in an emittance measurement, the following procedure is often used:

1. For each value of quadrupole field strength  $k$ , the wire is scanned and the amplitude of the response measured by a detector is obtained as a function of wire position.
2. For each wire scan at fixed  $k$ , the distribution is fit with a Gaussian of the form

$$f(x) = f_0 + f_{max} e^{-\frac{(x-f_0)^2}{2\langle x^2 \rangle}}, \quad (3.24)$$

where  $f_0$  is the baseline level offset and  $f_{max}$  is the peak value of the Gaussian distribution.

3. The fitted beam size  $\langle x^2 \rangle$  is plotted as a function of  $k$ .
4. The result is fit with a parabola. One parametrization for the fit is

$$\begin{aligned}\sigma_{11} &= A(k - B)^2 + C \\ &= Ak^2 - 2ABk + (C + AB^2).\end{aligned} \quad (3.25)$$

5. The  $\sigma$  matrix is reconstructed by equating coefficients:

$$A = S_{12}^2 \sigma_{11}, \quad (3.26)$$

$$-2AB = 2S_{11} S_{12} \sigma_{11} + 2S_{12}^2 \sigma_{12}, \quad (3.27)$$

$$C + AB^2 = S_{11}^2 \sigma_{11} + 2S_{11} S_{12} \sigma_{12} + S_{12}^2 \sigma_{22}, \quad (3.28)$$

and solve for  $\sigma_{11}$ ,  $\sigma_{12}$  ( $=\sigma_{21}$ ), and  $\sigma_{22}$ . The results are

$$\sigma_{11} = \frac{A}{S_{12}^2}, \quad (3.29)$$

$$\sigma_{12} = -\frac{A}{S_{12}^2} \left( B + \frac{S_{11}}{S_{12}} \right), \quad (3.30)$$

$$\sigma_{22} = \frac{1}{S_{12}^2} \left[ (AB^2 + C) + 2AB \left( \frac{S_{11}}{S_{12}} \right) + A \left( \frac{S_{11}}{S_{12}} \right)^2 \right]. \quad (3.31)$$

6. The beam emittance is then calculated from the determinant of the beam matrix  $\epsilon = \sqrt{\det \sigma}$  and the errors are propagated:

$$\det \sigma = \sigma_{11} \sigma_{22} - \sigma_{12}^2$$

$$= \frac{AC}{S_{12}^4} \quad (3.32)$$

so

$$\epsilon = \frac{\sqrt{AC}}{S_{12}^2}. \quad (3.33)$$

The above results also give the ellipse parameters  $\alpha$ ,  $\beta$ , and  $\gamma$ :

$$\beta = \frac{\sigma_{11}}{\epsilon} = \sqrt{\frac{A}{C}}, \quad (3.34)$$

$$\alpha = -\frac{\sigma_{12}}{\epsilon} = \sqrt{\frac{A}{C}} \left( B + \frac{S_{11}}{S_{12}} \right), \quad (3.35)$$

$$\gamma = \frac{1}{\epsilon} = \frac{S_{12}^2}{\sqrt{AC}} [AB^2 + C] + 2AB \left( \frac{S_{11}}{S_{12}} \right) + A \left( \frac{S_{11}}{S_{12}} \right)^2. \quad (3.36)$$

As a check, the ellipse parameters should satisfy  $\beta\gamma - 1 = \alpha^2$ .

An example of emittance measurements in the two transverse planes  $x$  and  $y$  is shown in Fig. 3.13. The graphics output shows the square of the measured beam size in  $\mu m^2$  as a function of the quadrupole field strength in  $(\frac{kG}{m})m$ . The first two rows in the text display show the measured emittance ( $\epsilon_j$ ) and the normalized emittance ( $\gamma\epsilon_j$ ) with  $j = x, y$ . The unit designation ‘‘M-R’’ denotes mm-mrad; for example, the measured normalized emittances are  $(3.0 \pm 0.4) \times 10^{-5}$  [m-rad] in  $x$  by  $(4.00 \pm 0.04) \times 10^{-6}$  [m-rad] in  $y$ .

### 3.2.2 Multiple Wire Measurement of Beam Emittance

The beam emittance may be measured (in many applications noninvasively) using 3 wire scanners if there are no coupling elements or using 4 wire scanners with coupling (in the latter case each wire scanner should be equipped with several wires oriented at different angles in the transverse plane,  $e.g.$ , a horizontal, a vertical and a  $45^\circ$  wire). The optimum wire locations for maximum sensitivity (without coupling) are such that the separation between wires correspond to a difference in betatron phase advance  $\Delta\psi$  of  $\frac{90^\circ}{N_m}$ , where  $N_m$  is the number of wires used in the measurement. Letting  $\sigma_i$  denote the measured  $\sigma_{11}$ 's for wire  $i$ , and considering the case of 4 wires, the matrix equation to be solved is

$$\begin{pmatrix} \sigma_1 \\ \sigma_2 \\ \sigma_3 \\ \sigma_4 \end{pmatrix} = \begin{pmatrix} c_1^2 & 2c_1s_1 & s_1^2 \\ c_2^2 & 2c_2s_2 & s_2^2 \\ c_3^2 & 2c_3s_3 & s_3^2 \\ c_4^2 & 2c_4s_4 & s_4^2 \end{pmatrix} \begin{pmatrix} \sigma_{11} \\ \sigma_{12} \\ \sigma_{22} \end{pmatrix} = M_0 \begin{pmatrix} \sigma_{11} \\ \sigma_{12} \\ \sigma_{22} \end{pmatrix} \quad (3.37)$$

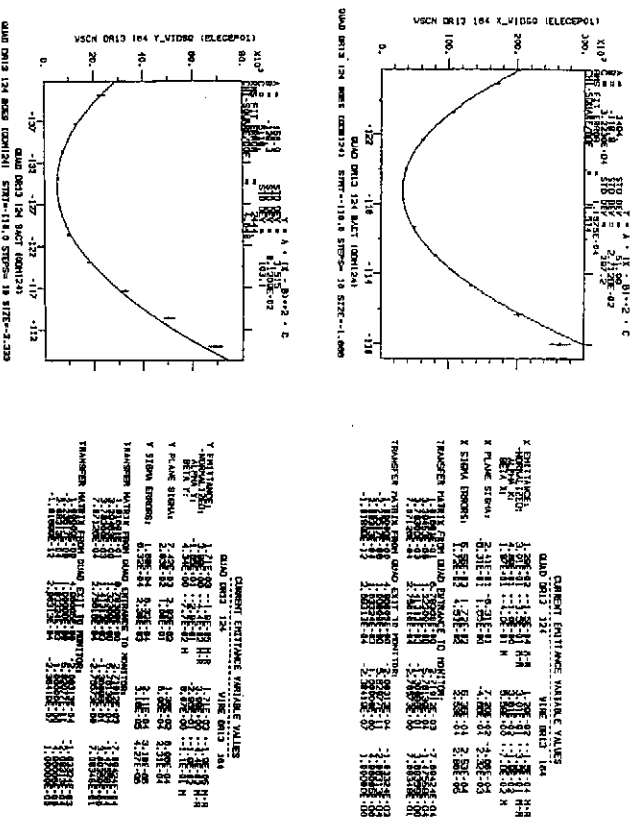


Figure 3.13: Example transverse beam emittance measurements using a single wire.

where  $c_i$  and  $s_i$  are the  $R_{11}$  and  $R_{12}$  transfer matrix elements from the point at which the beam matrix is defined to the location of the wire.

Notice that  $M$  need not be a square matrix. Rewriting Eq. (3.37) as  $A = MC$ , then  $M^T A = M^T M C$ , or  $C = (M^T M)^{-1} M^T A$ , that is,

$$\begin{pmatrix} \sigma_{11} \\ \sigma_{12} \\ \sigma_{22} \end{pmatrix} = (M^T M)^{-1} M^T \begin{pmatrix} \sigma_1 \\ \sigma_2 \\ \sigma_3 \\ \sigma_4 \end{pmatrix}, \quad (3.38)$$

which in a least-squares sense gives the beam matrix elements ( $\sigma_{ij}$ ) in terms of the measured sigmas.

A possible procedure for the multiple wire emittance measurement is as follows:

1. Each wire is scanned to obtain detector counts as a function of wire position  $x$ .
2. For each wire scan, the distribution is fit with a Gaussian using Eq. (3.24).
3. The  $\sigma$  matrix is reconstructed using Eq. (3.37), the transfer matrix elements  $M_i$  from the model, and the  $\sigma_i$  from the measurements.



4. The emittance is calculated  $\epsilon = \sqrt{\det \sigma}$ .
5. The ellipse parameters  $\alpha = -\frac{\sigma_{12}}{\epsilon}$ ,  $\beta = \frac{\sigma_{11}}{\epsilon}$ , and  $\gamma = \frac{\sigma_{22}}{\epsilon}$  are calculated, if desired.

### 3.2.3 Graphics

Increased operational efficiency may be obtained from meaningful graphical representation of the experimental data. In the multiple wire emittance measurement it is useful to project the measurements to a single point along the accelerator and to plot the normalized phase space. The emittance  $\epsilon$ , multiplied by  $\pi$ , corresponds to the area of the ellipse parametrized by

$$\epsilon = \gamma x^2 + 2\alpha x x' + \beta x'^2. \quad (3.39)$$

Since  $\beta\gamma = 1 + \alpha^2$ ,

$$\begin{aligned} \epsilon &= \frac{1}{\beta} [x^2 + (\alpha x + \beta x')^2] \\ &= \frac{1}{\beta} (x^2 + p_x^2), \end{aligned} \quad (3.40)$$

where  $p_x = \alpha x + \beta x'$  is the orthogonal coordinate to  $x$ .

A useful representation of the data may be obtained with the following procedure. In this representation, the data are shown in normalized phase space for direct viewing of deviations from design. The wire orientations are also plotted to show the phase space coverage by the wires.

1. Plot the design, rms ellipse in the phase space (a circle)

$$\left( \frac{x}{\sqrt{\beta}}, \frac{\alpha x + \beta x'}{\sqrt{\beta}} \right) \quad (3.41)$$

at some reference point  $s$  along the trajectory. Normalize the design ellipse to unit radius.

2. Plot also the ellipse obtained from the measurements of the ellipse parameters at the reference point. Apply same normalization as in step 1.
3. Using the lattice model, for each wire project its orientation back to the reference point and add the result to the figure; that is, for each point along the wire  $(x, x')_w$ , do an inverse mapping to the reference point

$$\begin{pmatrix} x \\ x' \end{pmatrix}_{\text{ref point}} = M^{-1} \begin{pmatrix} x \\ x' \end{pmatrix}_w. \quad (3.42)$$

The display should summarize the measurements which might include the measured and expected beam widths at each of the wires, the measured and design beam emittance, and the beam intensity. Also, a measure of the degree of "mismatch" is useful. This will be further discussed in the next section.

An example of these graphics is shown in Fig. 3.14. The raw data are given in Fig. 3.15. From Fig. 3.14 it is immediately obvious that while the measured ellipse has roughly the same emittance as the design circle (the horizontal emittance is  $208.8 \pm 9.9$  [mm-mrad] compared to the design of 200 [mm-mrad], the vertical emittance is  $323 \pm 26.7$  [mm-mrad] compared to the design of 200 [mm-mrad]), the ellipse orientation is incorrect. As will be shown in the next section, if this beam were allowed to propagate uncorrected, the final emittance would be  $390.0 \pm 10.2$  [mm-mrad] in  $x$  and  $543.3 \pm 13.2$  [mm-mrad] in  $y$ . The emittance dilution factor  $B_{mag}$  represents the degree of the mismatch. From Fig. 3.14 can be deduced immediately the degree of phase space coverage spanned by the wires. In the horizontal plane, for example, the wire orientations are about  $0^\circ$ ,  $-45^\circ$ ,  $-22.5^\circ$ , and  $-67.5^\circ$ , which is ideal for this 4-wire measurement from the SLC linac.

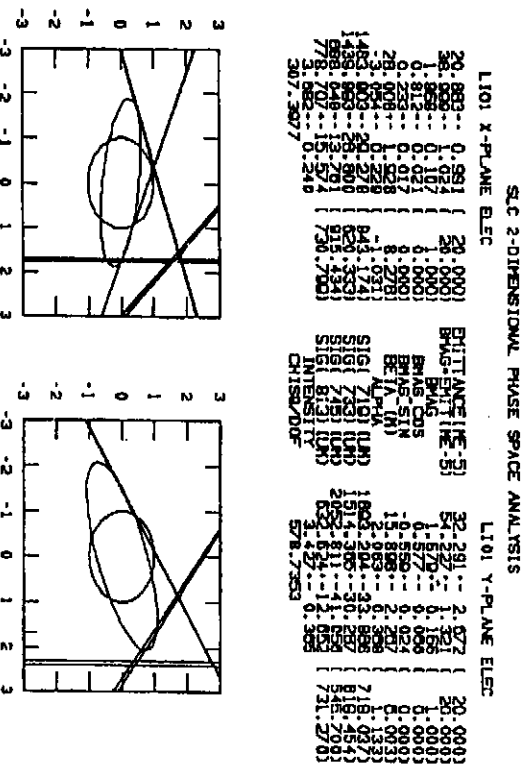


Figure 3.14: Graphics output of multiple wire transverse beam emittance measurement in the SLC linac.

The “measured ellipse”, that is the ellipse that was reconstructed from the individual wire scans based on the measured beam widths and the model-dependent transport matrices, does not represent in this case a true rms of the distribution as can be seen by inspection of the raw data shown in Fig. 3.15. For more complex beam distributions, a better characterization is achieved by using an “asymmetric Gaussian” distribution in which the left and right hand sides of the measured beam profile are fit

independently with two separate Gaussians. The fitting function<sup>26</sup> is

$$f(x) = f_0 + f_{max} e^{\left[ -\frac{(x-\langle x \rangle)^2}{2\langle x^2 \rangle (1 + \sigma | \sin(x-\langle x \rangle) |)} \right]} \quad (3.43)$$

where  $\alpha$  represents an asymmetry factor and is zero for a perfect Gaussian. The  $\sigma$  for the left and right hand sides of the fitted distribution are  $\sigma = \langle x^2 \rangle (1 \pm \alpha)$ . For the ellipse reconstruction the average  $\sigma$  was used. When large tails are present in the raw data this more accurately represents the beam distribution. Based on the raw data it is clear however that even with the more sophisticated fitting algorithm, the fit only marginally represents the actual distributions.

For reasonably well “matched” beams, the graphical summary display is most useful. In this example however, the raw data are more revealing: the “double-humps” in the raw data are characteristic of an upstream error; a beam, if kicked transversely will filament (lose coherency due to the natural spread in the phase advance) resulting in an increased emittance and the double-humps.

If a wire is mounted at 45° with respect to  $x$  and  $y$  (a “ $u$ -plane” wire), then it is also possible to measure the coupling between  $x$  and  $y$ . The full  $\sigma$ -matrix is

$$\sigma = \begin{pmatrix} \sigma_{11} & \sigma_{12} & \sigma_{13} & \sigma_{14} \\ \sigma_{21} & \sigma_{22} & \sigma_{23} & \sigma_{24} \\ \sigma_{31} & \sigma_{32} & \sigma_{33} & \sigma_{34} \\ \sigma_{41} & \sigma_{42} & \sigma_{43} & \sigma_{44} \end{pmatrix}, \quad (3.44)$$

where for example  $\sigma_{14}$  represents the coupling between  $x$  and  $y'$ . Notice that  $\sigma_{14} \neq \sigma_{23}$ . Whereas for the single plane, uncoupled beam matrix reconstruction a minimum of 3 measurements are required, to fully reconstruct the coupled beam matrix a total of 10 measurements is needed. This includes the 3 measurements in the  $x$  plane, 3 in the  $y$  plane, and 4 in the  $u$  plane. An example of a coupled emittance measurement is presented in Figs. 13-16. In this case the raw data are well fit by a Gaussian. In the text of Fig. 3.16, the parameters  $\epsilon_1$  and  $\epsilon_2$  represent the emittance one would measure in the absence of coupling. They are in good agreement with the measured projected emittances  $\epsilon_x$  and  $\epsilon_y$ , which indicates that, in this example, the coupling is small.

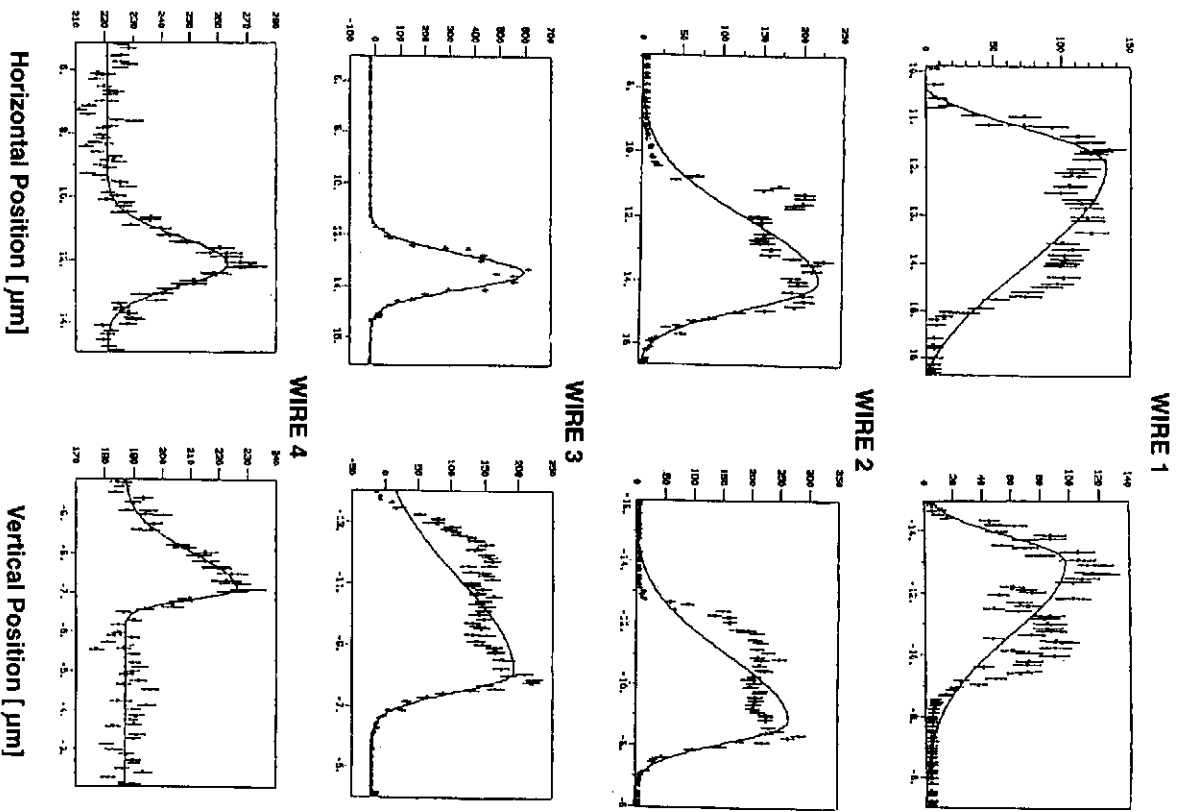


Figure 3.15: Raw data showing individual wire scans used in summary display of Fig. 3.14 and “asymmetric Gaussian” fits (cf. Eq. 3.43).

```

Four Dimensional Phase Space Analysis          L102 ELEC 2.9E10/bunch
-----
epsilon_x = 2.20          +-1.42E-02          epsilon_y = 1.89          +-1.72E-02
epsilon_b_x = 2.23          +-1.15E-02          epsilon_b_y = 1.95          +-2.05E-02
Bmag_x = 1.01          +-----+          Bmag_y = 1.03          +-3.03E-03
Bmag_cos_x = 6.355E-02          +-1.13E-02          Bmag_sin_y = 0.248          +-1.12E-02
Bmag_sin_x = 0.152          +-1.50E-02          beta_cos_y = 1.129          +-2.90E-02
beta_cos_x = 1.08          +-1.44E-02          beta_sin_y = 3.214E-02          +-1.37E-02
beta_sin_x = 0.154          +-0.00E+00          theta_2/deg = -12.6          +-0.00E+00
theta_1/deg = -11.8          +-0.00E+00          theta_4/deg = 11.7          +-0.00E+00
theta_3/deg = -20.5          +-0.00E+00          det C = -0.114          +-0.00E+00
tr(CCC) = 0.245          +-0.00E+00

epsilon_1 = 2.13          +-0.00E+00          epsilon_2 = 1.71          +-0.00E+00
-det G = 3.295E-02          +-0.00E+00          psi+/deg = -126.          +-0.00E+00
det G = 0.128          +-0.00E+00          psi-/deg = -89.4          +-0.00E+00
tr(BB) = 0.398          +-0.00E+00          det B = 0.104          +-0.00E+00

```

Figure 3.16: 4-dimensional emittance measurement summary.

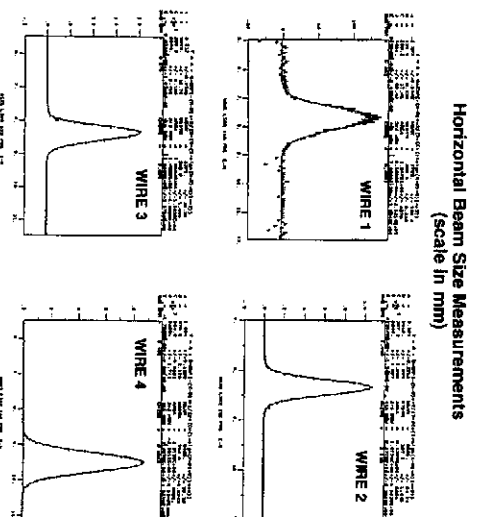


Figure 3.17: Raw data in  $x$ -plane corresponding to 4-D measurement of Fig. 3.16.

**Vertical Beam Size Measurements**  
(scale in mm)

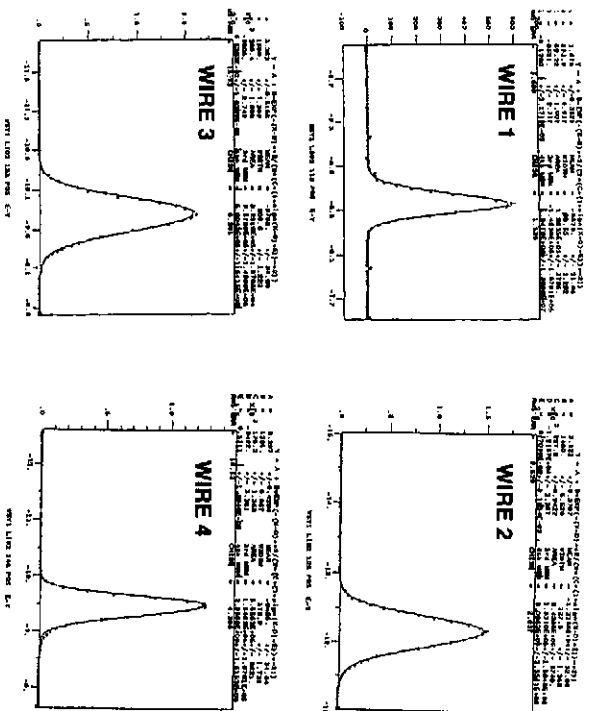


Figure 3.18: Raw data in  $y$ -plane corresponding to 4-D measurement of Fig. 3.16.

### "Skew" Beam Size Measurements (scale in mm)

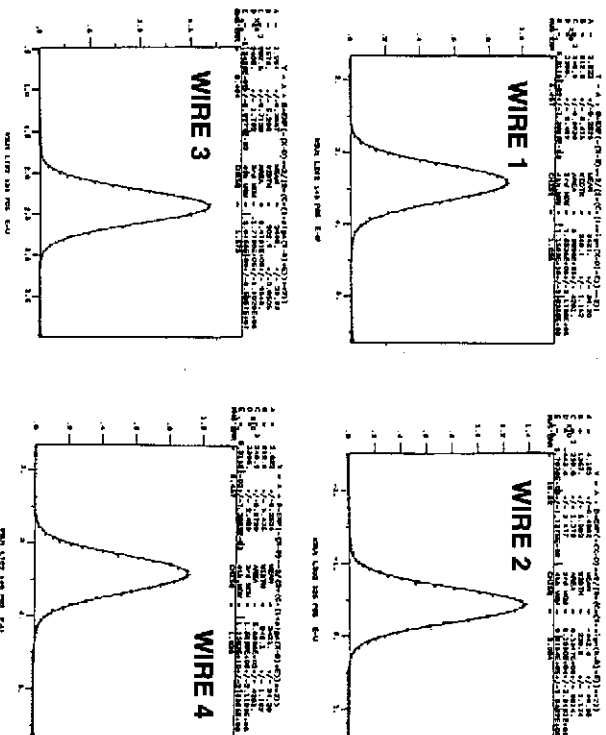


Figure 3.19: Raw data in  $x$ -plane corresponding to 4-D measurement of Fig. 3.16.